Dynamic and Static Quenching of Fluorescence by 1–4 nm Diameter Gold Monolayer-Protected Clusters

ARTICLE *in* THE JOURNAL OF PHYSICAL CHEMISTRY B · APRIL 2006

Impact Factor: 3.3 · DOI: 10.1021/jp057028n · Source: PubMed

6 AUTHORS, INCLUDING:

Debbie S. Silvester
Curtin University
55 PUBLICATIONS **1,634** CITATIONS

SEE PROFILE

Dynamic and Static Quenching of Fluorescence by 1−4 nm Diameter Gold Monolayer-Protected Clusters

Pearl Pui Hang Cheng,[†] Debbie Silvester,[‡] Gangli Wang,[§] Gregory Kalyuzhny, Alicia Douglas, and Royce W. Murray*

Department of Chemistry, Venable and Kenan Laboratories, University of North Carolina, CB#3290, Chapel Hill, North Carolina 27599

Received: December 2, 2005; In Final Form: January 17, 2006

How the efficiency of molecular quenching by Au nanoparticles depends on nanoparticle size is reported for (a) dynamic (collisional) quenching of four different fluorophores by three Au nanoparticles having similar protective layers but differing core diameters (1.1, 1.6, and 2.0 nm) and (b) static quenching in the electrostatic association between $[Ru(bpy)_3]^{2+}$ and five tiopronin-protected Au nanoparticles having core diameters from 1.3 to 3.9 nm. The quenching constants systematically increase with core size. In (a), the dynamic constants scale with the molar absorbance coefficients of the nanoparticles, showing the essentially of the absorbance/emission spectral overlap, and the associated nanoparticle core density of electronic states, in energy-transfer quenching. In (b), the fluorescence of the Au nanoparticle itself was enhanced by energy transfer from the $[Ru(bpy)_3]^{2+}$ fluorophore.

Introduction

Metal surfaces and metal films are well-known potent quenchers of molecular excited states. For example, in early work, Kuhn[1] demonstrated energy-transfer quenching of luminescent dyes spatially separated from Au films by well-defined Langmuir−Blodgett monolayers. Pagnot et al.[2] in a more recent, near-field optical microscopy study, described energy-transfer quenching by Au films.

Au nanoparticles are also quenchers of molecular luminescence, but this behavior is a newer and less quantitatively defined topic. There are at least three settings for quenching by unsupported, dissolved gold nanoparticles: (a) Binding a thiolated fluorophore to a Au nanoparticle has produced strong, structure-dependent "static" quenching of dansyl,[3] fluorenyl,[4] fullerene,[5] fluorescein,[6] lissamine dye,[7] and porphyrinic[8] fluorophores. Changes in quenching by MPCs of fluorophore labels involved in oligonucleotide hybridization[9] to its monolayer have been reported, with implications in chemical sensing. Luminescence enhancement, rather than quenching, can also occur, as by spatially controlled attachment leaving the molecular dipole parallel to the nanoparticle surface,[10] by aggregation effects,[11] and by suppression of nonradiative decay rates.[12] (b) Fluorophores can alternatively be reversibly bound, as by electrostatic interactions such as the interaction of cationic conjugated polymers[13] and the metal complex[14] $[Ru(bpy)_3]^{2+}$ with Au nanoparticles having anionic monolayer coatings. These situations produce strong static luminescence quenching and concurrent, weaker, collisional or "dynamic" quenching. (c) Quenching of molecular luminescence in solutions of fluorophores and nanoparticles that have no (obvious) binding affinity for one another occurs solely collisionally. We find, surprisingly, no published quantitative studies of the efficiency of collisional quenching by Au nanoparticles.

Our interest in quenching effects of metal nanoparticles is in the context of monolayer-protected Au clusters (MPCs).[15,16] The monolayers of MPCs are typically thiolate ligands, and the overall stability and synthetic flexibility of MPCs have allowed detailed analyses of composition and properties. It is particularly noteworthy that accessible sizes of the Au cores in MPCs cross the "metal-to-molecule" boundary. For example, thiolate-protected Au MPCs with core diameters from 0.8 to 2.1 nm and nuclearities of 10 to 22,[17a−d] 25,[17b] 28 or 29,[17b,e,f] 33,[17b] 38,[17g,h] 39,[17b] 75,[17i] 116,[17j,k] 140,[18] and 225[19] are known (albeit with quite widely varying stability and ease of synthetic access). All of these exhibit (or are anticipated to exhibit) size-dependent properties. For example, Au_{140} and Au_{225} MPCs (core diam 1.6 and 2.0 nm, respectively) have no obvious highest occupied molecular orbital−lowest unoccupied molecular orbital (HOMO−LUMO) energy gap but show[18,19] quantized double layer, single electron charging voltammetry. Au_{38} (diam 1.0 nm) and Au_{75} (diam 1.4 nm) MPCs display[17g,i] molecule-like HOMO−LUMO energy gaps in their electrochemical redox potentials and optical band edge absorbances, and the ligands become important contributors to properties. For example, electrochemical formal potentials of the $Au_{38}^{1+/0}$ MPC couple shift[20] with electron donating or withdrawing characteristics of *p*-substituents in thiophenolate monolayers, and near-infrared luminescence intensities of Au MPCs from Au_{38} to Au_{140} are more dependent on monolayer chemistry[21] than on nanoparticle size.[22]

How quenching of molecular luminescence depends on Au MPC nanoparticle size is the central focus of the present work. The existing quantitative evidence on size effects is limited but suggestive. Huang et al.[14] studied the aqueous solution quenching of $[Ru(bpy)_3]^{2+}$ luminescence caused by electrostatic binding to Au MPCs coated with *N*-(2-mercaptopropionyl)glycine (tiopronin) monolayers. The Stern−Volmer quenching constant (static constant $K_S = 1 \times 10^7\ M^{-1}$) of a 2.2 nm MPC was larger than that of a 1.8 nm diameter, tiopronin-coated MPC. The

* To whom correspondence should be addressed. E-mail: rwm@email.unc.edu.

[†] Present Address: Department of Chemistry, Bristol University, Bristol, U.K. (student).

[‡] Present address: Department of Chemistry, Oxford University, Oxford, U.K. (student).

[§] Present Address: Department of Chemistry, University of Utah, Salt Lake City, UT.

10.1021/jp057028n CCC: $33.50
Published on Web 02/15/2006

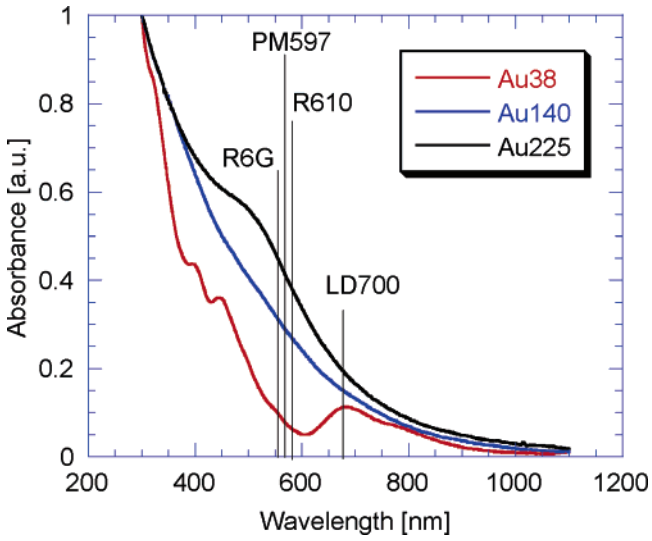

Figure 1. Absorbance spectra of Au38, Au140, and Au225 MPCs in 1:9 (vol/vol) CH_3CN/toluene and emission maxima (vertical lines) of fluorophores rhodamine 6G, PM597, rhodamine 610, and LD700. The spectra are normalized at 300 nm, for convenient comparison. The MPC molar absorbances are 6×10^3, 1.0×10^5, and 1.37×10^5 at 600 nm and 1.5×10^4, 6.1×10^4, and 7.4×10^4 cm^{-1} M^{-1} at 680 nm for Au38, Au140, and Au225, respectively.

energy-transfer quenching reported by Fan et al.[13] of conjugated polymers by 5, 10, and 20 nm citrate-coated Au MPCs was highly efficient, with K_S approaching 10^{11} M^{-1}. The quenching constant for a 2 nm Au nanoparticle was much smaller (10^7 M^{-1}). Dulkeith et al.[7] showed that the quenching of lissamine dye attached to a Au MPC involved both a size-dependent increase in nonradiative decay rate and a decrease in the radiative rate. The report by Ghosh et al.[23] on the size-dependent quenching of 1-methylaminopyrene fluorescence by 1−100 nm diameter, citrate-coated Au MPCs showed higher apparent quenching efficiencies with increasing nanoparticle size—although this was obscured in the report by an unfortunate choice of making comparisons at a common concentration of Au atoms (rather than at a common Au nanoparticle concentration). The collective evidence thus indicates that quenching efficiency increases for larger nanoparticles and offers partial explanations for it. However, what happens within the nanoparticle metal-to-molecule dimension regime has not been adequately penetrated, nor has the role of spectral overlap been addressed.

The present report describes two sets of steady-state fluorescence quenching experiments, within which MPC Au core size is varied. The quenched fluorophores differ in the two sets. The first set uses the series of nanoparticles[17g,18,19] $Au_{38}(SC_2Ph)_{24}$ (core diam 1.1 nm), $Au_{140}(SC_6H_{13})_{53}$ (diam 1.6 nm), and $Au_{225}(SC_6H_{13})_{57}$ (diam 2.0 nm), where SC_2Ph is phenylethylthiolate and SC_6H_{13} is hexanethiolate. These neutral, organic-soluble MPCs are abbreviated as Au38, Au140, and Au225, respectively. They have no functional binding sites and should accordingly act solely by collisional quenching, whose efficiency is measured by Stern−Volmer plots. The four quenched fluorophores (see Supporting Information, Figure S1 and Table S1) are the laser dyes pyrromethene 597 (PM597), LD700 perchlorate (LD700), rhodamine 610 perchlorate (rhodamine 610), and rhodamine 6G perchlorate (rhodamine 6G). The rhodamines absorb and emit in the range of 520−570 nm, wavelengths where the MPC absorbance spectra (Figure 1) are rather different. LD700 absorbs and emits at a lower energy, around 660 nm, where the smallest MPC (Au38) displays a weak absorbance maximum (660 nm) that the others do not. The fluorophores were thus chosen to probe the sensitivity of the collisional quenching process(es) to the differing electronic manifolds of the nanoparticles, that is, the spectral overlap of fluorophore emission and nanoparticle energy absorbance. The absorbance profile of course also reflects that of the density of electronic states.

The second set of experiments mirrors that of a previous[14] study (vide supra) but deploys a wider range of Au core dimensions (1.3−3.9 nm). The five tiopronin-coated Au MPCs, all somewhat polydisperse in core size, are referred to by their average diameters: 1.3, 1.8, 2.2, 3.1, and 3.9 nm Au tiopronin MPCs. The quenching of excited-state $[Ru(bpy)_3]^{2+*}$ luminescence by these MPCs is enhanced by electrostatic binding between the metal complex cation and the anionic MPCs in aqueous solution. The electrostatic binding is diminished by added electrolyte, the concentration of which is varied in a "quenching release" analysis as before.[14] $[Ru(bpy)_3]^{2+}$ was excited at 450 nm and emits at 610 nm. The absorbance spectra of these MPCs are relatively featureless, with absorbance climbing strongly as wavelength decreases (see Supporting Information). The larger ones display a superimposed, weak surface plasmon absorbance.

The results for both sets of MPCs reveal a clear increase in quenching efficiency (larger quenching constants) at increased MPC core size. In the first set, this could be identified as mainly governed by spectral overlap, or nanoparticle electronic density of states.

Experimental Section

Chemicals. PM597, LD700, rhodamine 6G, rhodamine 610, and rhodamine B base were purchased from Exciton (Dayton, Ohio). $HAuCl_4 \cdot 3H_2O$ was synthesized according to the literature.[24] House distilled water was purified with a Barnstead NANOpure system (18.3 MΩ). All other chemicals were reagent grade and used as received.

MPC Syntheses. The organic-soluble nanoparticles $Au_{38}(SC_2Ph)_{24}$, $Au_{140}(SC_6H_{13})_{53}$, and $Au_{225}(SC_6H_{13})_{57}$, where SC_2Ph is phenylethylthiolate and SC_6H_{13} is hexanethiolate, were synthesized according to a modified Brust[25] reaction, as described previously.[18a,19,26] The differences in ligands may exert a small effect on the fluorescence quenching, but they are of similar length; hexanethiolate-coated Au38 was not used because of stability limitations.[18c] These MPCs will be abbreviated as Au38, Au140, and Au225, respectively.

Synthesis of the water-soluble tiopronin-protected Au MPCs also followed a previous report.[27] Briefly, a (3:1 mol/mol ratio) thiol/Au reaction mixture of 2.0 g of $HAuCl_4 \cdot 3H_2O$ (5.1 mmol) with 2.5 g of tiopronin (*N*-(2-mercaptopropionyl)glycine, 15.3 mmol) in 125 mL of 6:1 methanol−acetic acid, stirred at 0 °C for 15 min, produced a ruby-red solution, which was reduced at 0 °C to a black solution by adding 3.8 g of $NaBH_4$ (100 mmol in 100 mL H_2O). After rapid stirring for 30 min, the solution was rotary evaporated (at <30 °C), and the MPCs were taken up into a minimum amount of water which after adjusting the pH to 1 with HCl was filtered and the solution diluted to about 230 mL. This solution was purified of small molecule impurities by dialysis (Specta/Por CE, MWCO = 8000 cellulose ester dialysis tubes, three sections, placed in 4 L beakers of slowly stirred Nanopure water) for 3 days, recharging with fresh water approximately every 10 h over the course of 72 h. The dialyzed solutions were filtered and the water removed by rotary evaporation (at <30 °C), yielding 0.97 g of solid MPC product. The product, according to identical previous[27] syntheses, has an average composition of $Au_{201}(tiop)_{85}$ and 1.8 ± 0.7 nm core diameter.

TABLE 1: Absorbance and Emission Maxima of Fluorophores and Their Dynamic Quenching Constants for Au38, Au140, and Au225 MPCs

fluorophore	absorbance/emission maxima, nm[a]	fluorophore concentration range, μM	$K_D \times 10^{-4}$, M^{-1}			relative K_D/ϵ[b]		
			Au38	Au140	Au225	Au38	Au140	Au225
PM597	528/567	0.45−1.02	7.4	48	180	1	0.4	1.1
LD700	652/676	0.39−0.56	10	39	130	1	0.2	0.35
rhodamine 6G perchlorate	532/554	0.61−0.77	29[c]	100	230	1	0.2	0.3
rhodamine 610 with acid	559/580	0.61	36	110	260	1	0.95	2.6

[a] Excitation wavelength was within a few nanometers of the absorbance maximum or at it. [b] ϵ (Beer's law absorbance coefficient, cm^{-1} M^{-1}) is 6×10^3, 1.0×10^5, and 1.37×10^5 at 600 nm and 1.5×10^4, 6.1×10^4, and 7.4×10^4 at 680 nm for Au38, Au140, and Au225, respectively. The K_D/ϵ values stated are relative to that for Au38. [c] The Stern−Volmer plot showed three segments of data; the number given corresponds to the slope of the lowest concentration segment.

Analogous preparations were carried out using 1:1, 1:6, and 1:12 thiol/Au mole ratios, which produce[27] MPCs with *average* compositions $Au_{314}Tio_{101}$ (diam 2.2 ± 1.0 nm), $Au_{1289}Tio_{126}$ (diam 3.1 ± 1.2 nm), and $Au_{2406}Tio_{268}$ (diam 3.9 ± 1.7 nm), respectively. A multiple-lane preparative gel electrophoretic fractionation (agarose gel, borate buffer) was conducted on 0.1 g of the 1.8 nm Au tiopronin MPC sample. Eight visible bands could be discerned after 4−5 h. To purify the MPC fractions from the gel materials, they were electrophoretically induced to migrate out of the gel slices into water. TEM of MPCs isolated from one of the faster moving gel fractions showed an average core size of 1.3 ± 0.2 nm, which suggests an average core Au_{75} MPC. It was assumed to have 40 tiopronin ligands by analogy to another[17i] Au_{75} MPC. The 2.2 nm Au tiopronin MPC sample was partially purified by a similar fractionation.

Spectroscopy. Fluorescence measurements were taken at standard right angle configuration on an ISA Instruments Jobin Yvon-Spex Fluorolog Model FL3-21 spectrometer, using a Hamamatsu R928 photomultiplier and 450 W xenon lamp source. The emission spectra were corrected for variation in the PMT spectral sensitivity. In studies of $[Ru(bpy)_3]^{2+}$ luminescence quenching, solutions were excited at 450 nm and spectra taken in the range 470−840 nm. UV−vis spectra were taken over 300−1100 nm with a Shimadzu 1601 UV−vis spectrophotometer.

Transmission Electron Microscopy (TEM). TEM of Au tiopronin MPC preparations was conducted with a side-entry Phillips CM12 electron microscope operating at 120 keV. TEM samples were prepared by spotting 5 μL of a dilute solution of MPC in water (~0.1 μM) on 3 mm copper grids (400 mesh). Phase-contrast images of the MPCs were obtained of typical regions on each MPC sample, at 380 000× or 510 000× magnification. Histograms of the Au core sizes were obtained from a digitized photographic enlargement using Scion Image software Beta Release 2 (www.scioncorp.com). Example TEM results are shown in Supporting Information Figures S2 and S3.

Solutions. Dynamic quenching of the fluorophore dyes with Au38, Au140, and Au225 MPCs was studied in acetonitrile/toluene (1:9 vol/vol, a mixture chosen for solubility purposes). The typical procedure involved adding 1−100 μL increments of an MPC solution to 3 mL of fluorophore solution, taking fluorescence and UV−vis spectra after each addition. Concentrations were chosen so that solution absorbance was <0.2, to avoid self-absorbance effects. Structures of the fluorophore dyes and wavelengths of their absorbance and emission maxima and of excitation are shown in Figure S1 and Table S1.

Quenching of $[Ru(bpy)_3]^{2+}$ luminescence was studied in aqueous solutions at ambient[28] (4.7) pH. The typical procedure involved adding 1−100 μL increments of either a Au tiopronin MPC or KCl solution to 2 mL of a $[Ru(bpy)_3]^{2+}$ solution containing a known concentration of KCl and MPC.

Results and Discussion

Collisional Quenching of Dye Fluorophores by Au38, Au140, and Au225. The Stern−Volmer relationship[29] between quencher concentration and fluorescence intensity is

$$\frac{\phi_0}{\phi} = \frac{F_0}{F} = 1 + \left(\frac{k_q}{k_e + k_d}\right)[C_Q] = 1 + K_D[C_Q] \qquad (1)$$

where ϕ_0 and F_0 are, respectively, quantum yield and emission intensity in the absence of quencher, ϕ and F are the same parameters but in the presence of quencher, and k_q, k_e, and k_d are the rates of quenching, emission, and deactivation, respectively, K_D is the Stern−Volmer quenching constant for collisional deactivation, and C_Q is the concentration of MPC quencher cores. Plots of F_0/F against MPC concentration should ideally be (a) linear, (b) have $F_0/F = 1$ intercepts, and (c) exhibit slopes of K_D expressing the efficiency of the quenching of the fluorophore excited state.

Absorbance and fluorescence spectra for mixtures of rhodamine 610 fluorophore and various concentrations of Au38 MPCs are shown in the top part of Figure 2. The absorbance spectra are accurate summations[30] of the dye and nanoparticle spectra, with the dye contributing the sharp peak at 560 nm and the nanoparticle contributing the absorbance envelope at higher and lower wavelengths. The fluorescence spectrum is solely that of the dye—the Au MPCs exhibit no luminescence at these energies—and its intensity steadily decreases as the MPC concentration increases. The lower part of Figure 2 shows the linear Stern−Volmer plots resulting for the Au38 data and from analogous data for Au140 and Au225 MPCs. The slopes obviously increase with MPC core size. The quenching constants K_D are given in Table 1, which shows that the quenching of rhodamine 6G fluorescence by Au225 MPCs is roughly 8-fold more efficient than that by Au38.

The spectra and Stern−Volmer plots (Figures S4 and S5) for quenching of the PM597 and LD700 fluorophores resemble those in Figure 2. A 2-fold increase in PM597 concentration produced an insignificant effect on the quenching plot (data not shown). Quenching results for rhodamine 6G (Figure S6) were also well-behaved, except for an anomalous increase in quenching seen at higher concentrations of Au38. The quenching constant for Au38 was taken from the linear segment at lower concentration.

Quenching constants for these fluorophores are reported in Table 1 and display an increase in K_D with MPC core size for all fluorophores. The correlation between increasing K_D and MPC size is discussed later.

Quenching of $[Ru(bpy)_3]^{2+}$ Luminescence by Au Tiopronin MPCs. Quenching of the 610 nm luminescence of the metal complex $[Ru(bpy)_3]^{2+}$ was measured in aqueous solutions of Au tiopronin-protected MPCs with 1.3, 1.8, 2.2, 3.1, and 3.9

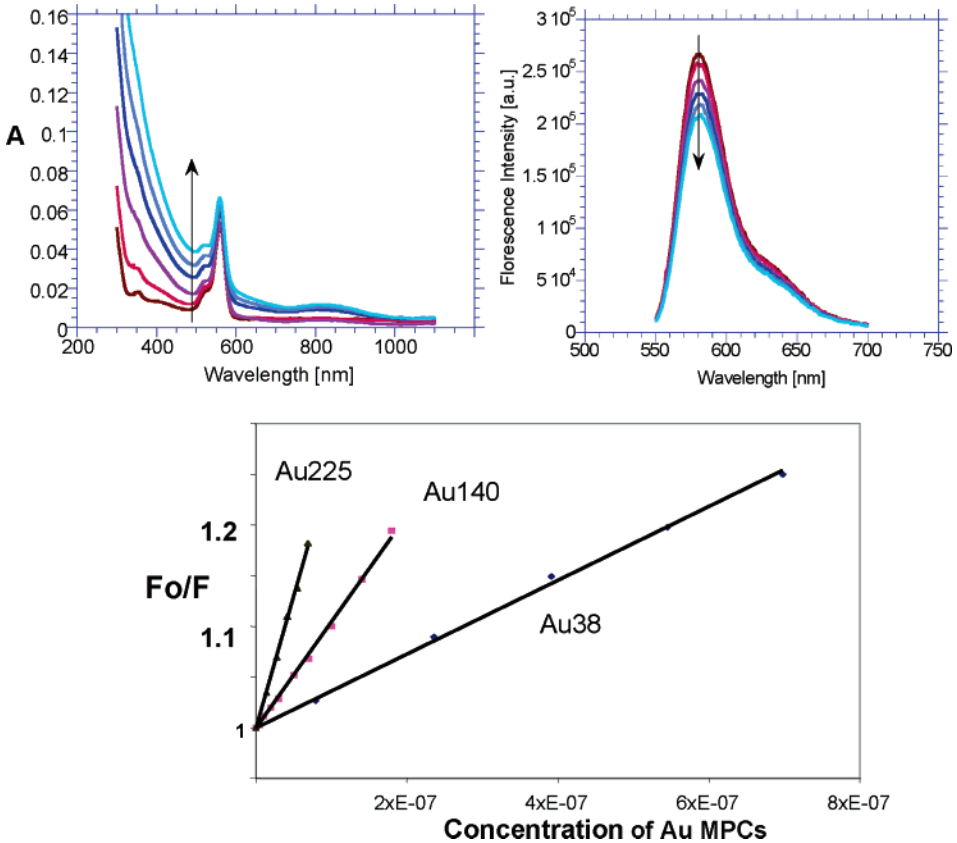

Figure 2. (upper) Absorbance (left) and fluorescence (right) spectra of rhodamine 610 (0.61 μM) in CH_3CN/toluene solution, (with added tosylic acid[30]), at Au38 concentrations of 0, 79, 240, 390, 550, and 700 nM, from bottom to top for absorbance and from top to bottom for fluorescence. (lower) Corresponding Stern−Volmer plots for rhodamine 610 (0.61 μM) for different concentrations of Au38, Au140, and Au225 MPCs. The best fit lines were drawn to pass through $F_0/F = 1$ at [MPC] = 0.

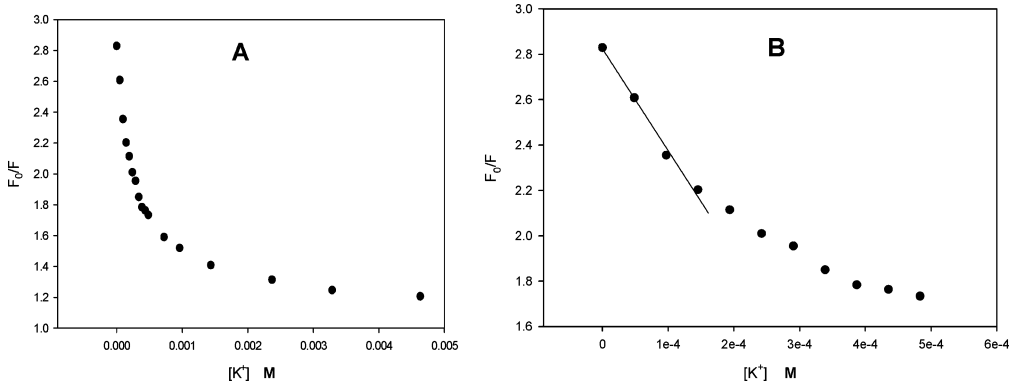

Figure 3. Quenching release plots for adding KCl electrolyte to aqueous solutions of 30 nM, 1.8 nm diameter, tiopronin-protected Au MPCs and 0.12 μM $[Ru(bpy)_3]^{2+}$ complex. Panel B is the low concentration part of panel A.

nm core diameters. The $[Ru(bpy)_3]^{2+}$ complex is used here at concentrations (μM) much greater than the added MPC quencher concentration (nM, unlike the previous study[14]), so as to maximize the extent of electrostatic binding between the two solutes. In solutions where $[Ru(bpy)_3]^{2+} \gg$ [MPC], the quenching of excited-state $[Ru(bpy)_3]^{2+}*$ is extensive but becomes sharply decreased by the addition of less than millimolar concentrations of KCl electrolyte since the added salt screens the carboxylate binding sites. We exploit this dependency to obtain "static" quenching constants of metal complex/MPC electrostatic binding, by measuring luminescence as a function of $[K^+]$.

With no added KCl, the luminescence quenching of an ~0.12 μM $[Ru(bpy)_3]^{2+}$ solution by 30 nM Au tiopronin MPCs (1.8 nm diam) is nearly 70%, as shown in Figure 3, panel A (0 mM K^+). Figure 4, panel A, shows that a larger MPC core (3.1 nm diam) produces an even stronger (>80%) quenching effect at even lower MPC concentration (14 nM).

The quenching is strongly released by adding less than millimolar concentrations of KCl electrolyte, as seen in Figures 3 and 4. The electrolyte effect is modeled in terms of a competition between formation of electrostatic complexes between $[Ru(bpy)_3]^{2+}$ and carboxylate groups of the MPC tiopronin monolayer shell

$$[Ru(bpy)_3]^{2+} + Au - tiop^- \leftrightarrow [Ru(bpy)_3^{2+}]\cdot[Au - tiop^-] \quad (2)$$

and analogous association with K^+

$$K^+ + Au - tiop^- \leftrightarrow [K^+]\cdot[Au - tiop^-] \quad (3)$$

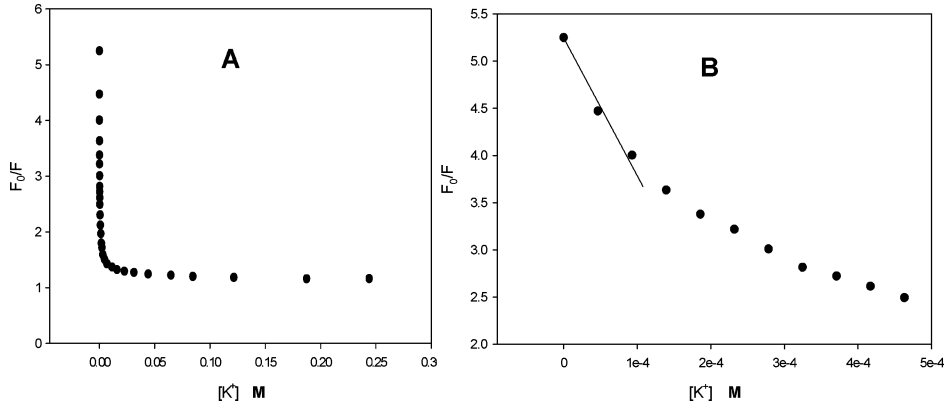

Figure 4. Quenching release plots for adding KCl electrolyte to aqueous solutions of 14 nM, 3.1 nm diameter, tiopronin-protected Au MPCs and 0.12 μM $[Ru(bpy)_3]^{2+}$ complex. Panel B is the low concentration part of panel A.

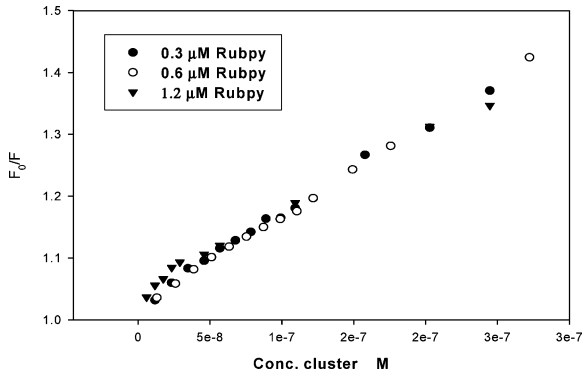

Figure 5. Stern−Volmer plots of eq 4 for dependency of quenching on MPC concentration, at 0.3, 0.6, and 1.2 μM $[Ru(bpy)_3]^{2+}$ concentrations in aqueous 0.15 M KCl. The averages of fitting the three sets of data to the equation are $K_D = 3.5\ (\pm\ 1.8) \times 10^5\ M^{-1}$ and $K_S = 1.8\ (\pm\ 0.3) \times 10^6\ M^{-1}$.

TABLE 2: Static and Dynamic Quenching Constants (K_S, K_D) and Electrolyte Binding Constants (K_M) as a Function of Tiopronin-Protected Au MPC Core Size

average core size, nm[a]	approx. K_D, M^{-1} [b]	K_S, M^{-1} [c]	K_M, M^{-1} [c]
1.3 ± 0.2	2×10^6	1.0×10^7	1×10^4
1.8 ± 0.7	3.5×10^5	5.9×10^7	2×10^4
2.2 ± 1.0	2×10^5	1.0×10^8	3×10^4
3.1 ± 1.2	2×10^6	3.1×10^8	4×10^4
3.9 ± 1.7	2×10^6	4.2×10^8	5×10^4

[a] On the basis of TEM observations. [b] K_D assessed from Stern−Volmer plots at high (0.15 M) [KCl], like Figure 5. [c] K_S and K_M taken from quenching release plots at lowest [KCl], like Figures 3 and 4.

Collisional as well as static quenching may occur; a Stern−Volmer equation accounting for both static and dynamic (collisional) quenching is[29]

$$\frac{F_0}{F} = 1 + (K_S + K_D)[C_Q] + K_S K_D [C_Q]^2 \qquad (4)$$

where K_S and K_D are static and dynamic quenching constants, respectively, and $[C_Q]$ is the concentration of a MPC quencher. Since we expect that $K_D < K_S$, K_D was estimated in quenching experiments at large [KCl] where the relative extent of static quenching is suppressed. Figure 5 shows that there quenching is independent of $[Ru(bpy)_3]^{2+}$ concentration, which is expected since it is much greater than the MPC concentration. The K_D values obtained (Table 2) from the fitting of eq 4 to data like Figure 5 for the different size MPCs are rather approximate, but this is of no consequence in the assessment of static quenching (K_S) at low [KCl], where static quenching is the larger effect.

At lower MPC concentrations, eq 1 can be written

$$\frac{F_0}{F} = 1 + K_D[C_Q] + K_S[C_Q]_{ACTIVE} \qquad (5)$$

where $[C_Q]_{ACTIVE}$ represents the concentration of carboxylate binding sites on the MPCs tiopronin monolayer shell that are available as electrostatic binding sites for $[Ru(bpy)_3]^{2+}$

$$[C_Q]_{ACTIVE} = \left(\frac{N[C_Q]K_a}{K_a + [H]^+}\right)\left(\frac{1}{1 + K_M'[M]}\right) \qquad (6)$$

This expression corrects the total MPC concentration $[C_Q]$ (a) for the number (N) of tiopronin ligands and carboxylic acid groups per MPC (for example, 85 for the 1.8 nm MPC), (b) for their fractional dissociation at pH 4.7 (the $K_A/(K_A+[H^+])$ term, where $pK_A = 5.7$[27]), and (c) for the fraction of carboxylates that are bound to the K^+ ion (the $1/(1 + K_M'[M])$ term, where K_M' is the (carboxylic acid dissociation-corrected) association constant of eq 3 and [M] is $[K^+]$). For the 1.8 nm MPCs, assuming that $1 > K_M'[M]$ and inserting the appropriate parameters, leads from eqs 5 and 6 to

$$\frac{F_0}{F} = 1.06 + 3.0 \times 10^{-8} K_S - 3.8 \times 10^{-9} K_S K_M'[M] \qquad (7)$$

Analogous equations for the other MPC sizes are given in Table S2 in the Supporting Information. These equations are used in the analysis of "quenching release" plots of F_0/F against [M] (where $M = K^+$), to determine values of the static constant K_S.

In the above quenching model, which is the same as that employed earlier,[14] the value of K_S represents the combined extent of equilibrium association of $[Ru(bpy)_3]^{2+}$ with MPC and the degree of quenching, once associated. The latter property may also reflect relative values of the fluorophore excited-state lifetime and the exchange dynamics of eq 2. The model offers the advantage that the degree of static quenching, as modified by competition between the reactions in eqs 2 and 3 above, can be assessed from the slopes and intercepts of quenching release plots of F_0/F against added $[K^+]$. Such plots are curved at higher $[K^+]$, as seen in the typical Figures 3 and 4, since K_S decreases as the overall fraction of $[Ru(bpy)_3]^{2+}$ complexes bound to the tiopronin-coated MPCs decreases at higher $[K^+]$. Using slopes and intercepts of the plots over the lowest ranges of $[K^+]$ (up to about 10^{-4} M, Figures 3B and 4B) gives the K_S

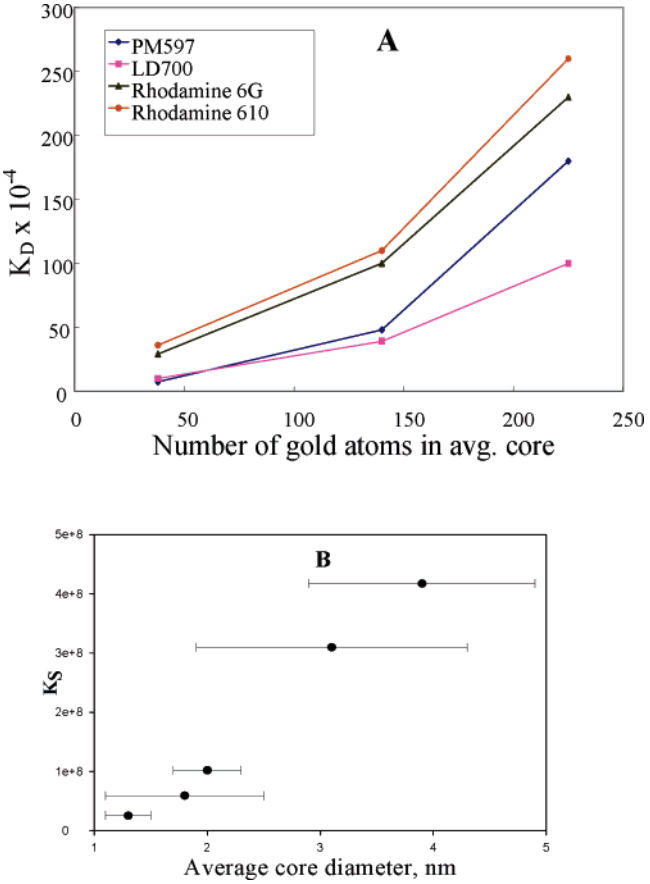

Figure 6. (a) Dynamic quenching constants (K_D) vs the number of Au core atoms for MPCs Au38, Au140, and Au225 and the indicated fluorophores, from Stern−Volmer plots as in Figure 2. (b) Static quenching constants (K_S) vs average core diameter (the error bars are from TEM characterization) obtained from quenching release experiments at low [KCl] in aqueous 0.12 μM $[Ru(bpy)_3]^{2+}$ solution.

and K_M results for the different MPC core sizes shown in Table 2. The K_S values are larger than those in the previous study[14] because the present experiments accessed lower [KCl] concentrations, where stronger electrostatic association enhanced the static quenching component.

Table 2 shows that both K_S and K_M increase with increasing MPC core size. The value of K_S for the 2.2 nm tiopronin MPC is about 4-fold larger than that for the 1.3 nm MPC, a difference in magnitude comparable to that in Table 1 for a similar core size change.

Relation of Quenching to MPC Core Size and Optical Absorbance. As noted in the Introduction, a central target of this study was to evaluate the core size dependency of the efficiency of the MPCs as quenchers. The results in Tables 1 and 2, plotted in Figure 6 against the numbers of core atoms and core diameters, respectively, show that *both* dynamic (upper panel) and static (lower panel) quenching are enhanced by larger nanoparticle cores. The effect of increasing size on static quenching (Figure 6B) is qualitatively consistent with the limited existing static quenching data on the $[Ru(bpy)_3]^{2+}$ system[14] and with other size-dependency static quenching results.[7,13,23] The dynamic quenching size dependency in Figure 6A is apparently the first quantitative observation based on collisional quenching.

Energy transfer is the most likely dominant mode of excited-state quenching in these experiments. The redox chemistries of the MPC nanoparticles have been well characterized;[17i,17g,18a] that of the four fluorophores has not, but from their disparate structures (Supporting Information Figure S1), one does not expect similarities in redox behavior. As a consequence of the latter, and of the lack of large differences between quenching constants of different fluorophores (at given MPC sizes), significant participation of electron-transfer quenching seems unlikely.

Multiple parameters[16] are known to influence the radiative and nonradiative decay kinetics of excited states near metal nanoparticles. Both decrease in the former and increase in the latter can occur[17] concurrently in a quenching situation. The parameters include[16] shape and size of the nanoparticle, distance between the excited-state molecule and nanoparticle surface, orientation of the molecular dipole with respect to the nanoparticle surface plane, and overlap of the molecule's emission spectrum with the nanoparticle's absorbance profile. Thiolate-capped Au_{38} and Au_{140} MPCs are predicted by theory[31] to have truncated octahedral nanocrystalline forms, so change in shape is not expected to be a factor. The separation between MPC core surface and fluorophore (upon collision) is constrained by the thickness of the capping monolayer, which for all the MPCs (Au38, Au140, and Au225) is about 0.8 nm. The distance is slightly longer for the tiopronin monolayers on their MPCs. Changes in quenching in the two MPC series cannot readily be attributed to changes in quencher−fluorophore distance, and the short distances should enable strong dipolar coupling between the fluorophore and metal nanoparticle. There is, finally, no designed control over the orientation[10] of the fluorophore molecular dipole relative to the MPC core surface.

As shown in Figure 1, the Au38, Au140, and Au225 absorbance spectra are quite different. Energy-transfer quenching is classically expected to be strongly influenced by the spectral overlap of fluorophore emission and quencher absorption. Such overlap can be assessed quantitatively by comparing quenching constants to molar absorbances[32] ϵ. The spectral envelopes of Au38, Au140, and Au225 MPCs (Figure 1, normalized at 300 nm) are similar at 680 nm but differ around 600 nm. The actual molar absorptivities of the three nanoparticles (see values in Figure 1 legend) are even more different: ϵ for Au38 at 600 nm is, for example, 20-fold smaller than that for Au225. The emission wavelengths of three of the fluorophores all lie near 600 nm (ignoring the small differences in their emission wavelengths).

The role of spectral overlap is examined in Table 1, right, by asking whether the dynamic quenching constants for the fluorophores *scale with the absorbance coefficients*, ϵ. This comparison is done in terms of K_D/ϵ ratios, which are stated relative to that for Au38. It is remarkable that the K_D/ϵ ratios at 680 nm (for LD700) are the same, within a factor of <3-fold, that is, the variation of K_D with MPC core size roughly mirrors the differences between molar absorbances of the MPC cores at 680 nm. At 600 nm, where the molar absorptivities of the MPCs vary even more widely, the K_D values for the other three fluorophores track the values of ϵ even more impressively. The variations among Au38, Au140, and Au225 are even smaller if one considers the differences in collision rates in solution expected from their different hydrodynamic diameters. On the basis of the 1.1, 1.6, and 2.0 nm diameters (core and monolayer) for Au38, Au140, and Au225, respectively, Au38 should diffuse about 1.3-fold faster than Au225, for example.

The correlation between K_D and ϵ in Table 1 is obviously crude, but considering the similar behavior of four different fluorophores with different structural features, this amounts to an impressive case for the essentiality of spectral overlap in energy-transfer efficiency. While minor effects on K_D might arise from other factors, the comparison in Table 1 points out

the importance of the density of MPC core electronic states (DOS) in energy-transfer quenching. The DOS should of course scale with values of ϵ. This furthermore means that K_D is not expected to simply scale only with a nanoparticle cross-section or surface area but also with how the optical absorbance changes with nanoparticle size.

Somewhat surprisingly, it does not seem to greatly matter that Au38 is a molecule-like nanoparticle, with a HOMO−LUMO energy gap, which the other MPCs lack. On the other hand, the fluorophore excited-state energies transferred lie at higher values than those so far mapped out in the energy level structure of Au38 and may perhaps be less discretized than those near the HOMO−LUMO energy gap of Au38.

The preceding analysis provides an explanation for the dependency of quenching on MPC core size shown in Figure 6A. The molar absorptivities of the MPCs increase with the number of Au atoms in their cores and accordingly the core DOS, and because of that, *the larger MPCs are progressively more efficient collisional quenchers*. We anticipate this as a general result for dynamic quenching by nanoparticles, at least in cases where molecular dipole orientations are intrinsically uncontrolled with respect to the nanoparticle surface and where similar distances—determined by a capping layer—separate the nanoparticle core from the excited-state fluorophore.

We are unable to provide a similar quantitative spectral overlap analysis for the quenching of the metal complex $[Ru(bpy)_3]^{2+}$ fluorescence by Au tiopronin-protected MPCs. That set of experiments employed only a single fluorophore, and the spectral envelopes of the different nanoparticles are similar (Figure S7). The similarity of the scale of changes in K_S in Figure 6B and of K_D in Figure 6A leads us, however, to speculate that the spectral overlap and increase in values of ϵ with nanoparticle size are again the dominant sources of the size dependency of the quenching and quenching efficiency is expected to scale with molar absorbance coefficient. One must, however, keep in mind that our scheme for assessing static quenching convolves it with a binding constant (eq 2) and the ligand coverage per nanoparticle (eq 6). K_S does scale roughly with the number of tiopronin ligands, except for the smallest nanoparticle.

Concurrent Quenching and MPC Emission Observations. The tiopronin-protected 1.8 nm Au MPCs exhibit emission that is observable at long wavelengths in the visible region and which extend strongly into the near-infrared region.[22] Measurements of the tiopronin MPC emission at 770 nm in the absence of the $[Ru(bpy)_3]^{2+}$ complex show a linear relation between emission intensity and concentration over nanomolar concentrations (Figure 7, lower, ●).

Figure 7 (upper) shows an experiment in which a 1.8 nm core diameter MPC was incrementally added to a 0.6 μM $[Ru(bpy)_3]^{2+}$ solution in concentrations up to about 100 nM. The $[Ru(bpy)_3]^{2+}$ emission intensity falls, as expected from the above discussion, and concurrently, MPC emission intensity grows at 770 nm. An interesting aspect of the Figure 7 (upper) spectra is the appearance of an isosbestic point (indicated). This shows that the quenching of an increment of $[Ru(bpy)_3]^{2+}$ luminescence is accompanied nearly 1:1 by the appearance of an increment of luminescing tiopronin MPC in the solution. Further, Figure 7 (lower) shows that, as compared to solutions in which $[Ru(bpy)_3]^{2+}$ is absent (● data), the presence of $[Ru(bpy)_3]^{2+}$ *enhances* the MPC emission intensities (o data) by roughly 40%. This effect implies a photosensitization of MPC luminescence by the energy transfer from $[Ru(bpy)_3]^{2+}$. This is unsurprising given that the energy transfer and emission is downhill, energy-wise. Energy transfers between attached fluorophores and carbon nanotubes and Au nanoparticles have been encountered previously,[33,34] but the phenomenon is not yet fully explored.

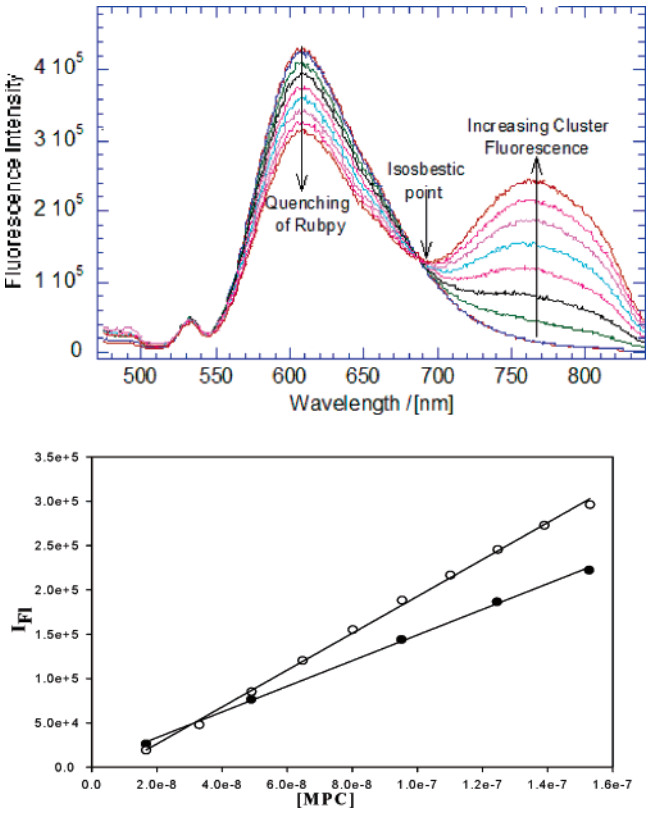

Figure 7. (upper) Fluorescence spectra of aqueous solutions of 0.6 μM $[Ru(bpy)_3]^{2+}$ to which tiopronin-protected, 1.8 nm core diameter Au MPCs are added at concentrations of 0, 17, 33, 49, 65, 95, 110, and 124 nM. (lower) MPC emission intensity at 770 nm as a function of [MPC] in the presence (○) and absence (●) of 0.6 μM $[Ru(bpy)_3]^{2+}$.

Acknowledgment. This research was supported in part by grants from the National Science Foundation and the Office of Naval Research. The authors thank Wei Wang, Rui Guo, and Rebecca Wolfe of UNC-CH, for gifts of synthesized Au38, Au140, and Au225 MPCs, respectively.

Supporting Information Available: Figure and table giving structural and emission details for fluorescent dyes. Figures showing TEM images, histograms, and absorbance spectra for tiopronin-coated MPCs. Stern−Volmer plots for PM597, LD700, and rhodamine 6G. Table giving K_D, C_Q, and individual eqs for different cluster sizes. Further background information and experimental details are also given. This material is available free of charge via the Internet at http://pubs.acs.org.

References and Notes

(1) Inacker, O.; Kuhn, H. *Chem. Phys. Lett.* **1974**, *27*, 317−321.
(2) Pagnot, T.; Barchiesi, D.; Tribillon, G. *Appl. Phys. Lett.* **1999**, *75*, 4207−4209.
(3) Aguila, A.; Murray, R. W. *Langmuir* **2000**, *16*, 5949−5954.
(4) Gu, T.; Whitesell, J. K.; Fox, M. A. *Chem. Mater*. **2003**, *15*, 1358−1633.
(5) Sudeep, P. K.; Ipe, B. I.; Thomas, K. G.; George, M. V.; Barazzouk, S.; Hotchandani, S.; Kamat, P. V. *Nano Lett.* **2002**, *2*, 29.
(6) Templeton, A. C.; Cliffel, D. E.; Murray, R. W. *J. Am. Chem. Soc.* **1999**, *121*, 7081.
(7) Dulkeith, E.; Morteani, A. C.; Niedereichholz, T.; Klar, T. A.; Feldmann, J.; Levi, S. A.; van Veggel, F. C. J. M.; Reinhoudt, D. N.; Motter, M.; Gittens, D. I. *Phys. Rev. Lett.* **2002**, *89*, 203002/1−4.

(8) Imahori, H.; Kashiwagi, Y.; Endo, Y.; Hanada, T.; Nishimura, Y.; Yamazaki, I.; Araki, Y.; Ito, O.; Fukuzumi, S. *Langmuir* **2004**, *20*, 73−81.

(9) (a) Dubertret, B.; Calame, M.; Libchaber, A. J. *Nat. Biotech.* **2001**, *19*, 365−370. (b) Maxwell, D. J.; Taylor, J. R.; Nie, S. *J. Am. Chem. Soc.* **2002**, *124*, 9606−9612.

(10) (a) Hernandez, F. E.; Yu, S.; Garcy'a, M.; Campiglia, A. D. *J. Phys. Chem. B* **2005**, *109*, 9499−9504. (b) Thomas, K. G.; Kamat, P. V. *J. Am. Chem. Soc.* **2000**, *122*, 2655−2656.

(11) Zhang, J.; Malicka, J.; Gryczynski, I.; Lakowicz, J. R. *Anal. Biochem.* **2004**, *330*, 81−86.

(12) Thomas, K. G.; Kamat, P. V. *J. Am. Chem. Soc.* **2002**, *122*, 2655−2656.

(13) (a) Fan, C.; Wang, S.; Hong, J. W.; Bazan, G. C.; Plaxco, K. W.; Heeger, A. J. *PNAS* **2003**, *100*, 6297−6301. (b) Gaylord, B. S.; Wang, S.; Heeger, A. J.; Bazan, G. C. *J. Am. Chem. Soc.* **2001**, *123*, 6417−6418.

(14) Huang, T.; Murray, R. W. *Langmuir* **2002**, *18*, 7077−7081.

(15) Templeton, A. C.; Wuelfing, W. P.; Murray, R. W. *Acc. Chem. Res.* **2000**, *33*, 27−36.

(16) Daniel, M.-C.; Astruc, D. *Chem. Rev.* **2004**, *104*, 293−346.

(17) (a) Woehrle, G. H.; Warner, M. G.; Hutchison, J. E. *J. Phys. Chem. B* **2002**, *106*, 9979. (b) Negishi, U.; Nobusada, K.; Tsukuda, T. *J. Am. Chem. Soc.* **2005**, *127*, 5261−5270. (c) Negishi, I.; Tsukuda, T. *J. Am. Chem. Soc.* **2003**, *125*, 4046. (d) Negishi, Y.; Takasugi, Y.; Sato, S.; Yao, H.; Kimura, K.; Tsukuda, T. *J. Am. Chem. Soc.* **2004**, *126*, 6518. (e) Schaaff, T. G.; Knight, G.; Shafigullin, M. N.; Borkman, R. F.; Whetten, R. L. *J. Phys. Chem. B* **1998**, *102*, 10643. (f) Link, S.; El-Sayed, M. A.; Schaaff, T. G.; Whetten, R. L. *Chem. Phys. Lett.* **2002**, *356*, 240. (g) Lee, D.; Donkers, R. L.; Wang, G.; Harper, A. S.; Murray, R. W. *J. Am. Chem. Soc.* **2004**, *126*, 6193. (h) Jimenez, V. L.; Georganopoulou, D. G.; White, R. J.; Harper, A. S.; Mills, A. J.; Lee, D.; Murray, R. W. *Langmuir* **2004**, *20*, 6864. (i) Balasubramanian, R.; Guo, R.; Mills, A. J.; Murray, R. W. *J. Am. Chem. Soc.* **2005**, *127*, 8126−8132. (j) Alvarez, M. M.; Khoury, J. T.; Schaaff, T. G.; Shafigullin, M.; Vezmar, I.; Whetten, R. L. *Chem. Phys. Lett.* **1997**, *266*, 91. (k) Schaaff, T. G.; Shafiguillin, M. N.; Khoury, J. T.; Vezmar, I.; Whetten, R. L.; Cullen, W. G.; First, P. N.; Gutierrez-Wing, C.; Ascensio, J.; Jose-Yacaman, M. J. *J. Phys. Chem. B* **1997**, *101*, 7885.

(18) (a) Hicks, J. F.; Miles, D. T.; Murray, R. W. *J. Am. Chem. Soc.* **2002**, *124*, 13322. (b) Quinn, B. M.; Liljeroth, P.; Ruiz, V.; Laaksonen, T.; Kontturi, K. *J. Am. Chem. Soc.* **2003**, *125*, 6644−6645. (c) Jimenez, V. L.; Georganopoulou, D. G.; White, R. J.; Harper, A. S.; Mills, A. J.; Lee D.; Murray, R. W. *Langmuir* **2004**, *20*, 6864−6870.

(19) Wolfe, R. L.; Murray, R. W. *Anal. Chem.*, submitted for publication.

(20) Guo, R.; Murray, R. W. *J. Am. Chem. Soc.* **2005**, *127*, 12140−12143.

(21) Kalyuzhny, G.; Guo, R.; Choi, J.-P.; Murray, R. W. UNC-CH, Chapel Hill, NC, Unpublished work, 2005.

(22) Wang, G.; Huang, T.; Murray, R. W.; Menard, L.; Nuzzo, R. G. *J. Am. Chem. Soc.* **2005**, *127*, 812−813.

(23) Ghosh, S. K.; Pal, A.; Kundu, S.; Nath, S.; Pal, T. *Chem. Phys. Lett.* **2004**, *395*, 366−372.

(24) a) *Handbook of Preparative Inorganic Chemistry*; Brauer, G., Ed.; AP: New York, 1965, p 1054. (b) Block, B. P. *Inorg. Synth.* **1953**, *4*, 14.

(25) Brust, M.; Walker, M.; Bethell, D.; Schiffrin, D. J.; Whyman, R. *J. Chem. Soc., Chem. Commun.* **1994**, 801−802.

(26) Donkers, R. L.; Lee, D.; Murray, R. W. *Langmuir* **2004**, *20*, 1945−1952.

(27) Huang, T.; Murray, R. W. *Langmuir* **2002**, *18*, 7077−7081.

(28) The solutions are buffered by atmospheric CO_2, at pH ∼4.7. The concentration of MPC acid groups in the nanomolar MPC solutions is too small to affect the pH. In the absence of added electrolyte, the apparent pK_a of Au tiopronin MPCs is[27] ∼5.7, so the carboxylic acid groups will be ∼10% dissociated in electrolyte and $[Ru(bpy)_3]^{2+}$ complex-free solutions.

(29) (a) Lakowicz, J. R. *Principles of Fluorescence Spectroscopy*; Plenum Press: New York, 1983. (b) Keizer, J. *J. Am. Chem. Soc.* **1983**, *105*, 1494−1498. (c) Turro, N. J. *Modern Molecular Photochemistry*; Benjamin, W. A.: New York, 1978. (d) Sharma, A.; Schulman, S. G. *Introduction to Fluorescence Spectroscopy*; Wiley-Interscience: New York, 1999.

(30) The rhodamine 610 solutions were acidified to suppress dissociation of the rhodamine 610 acid group; the absorbance spectra were otherwise anomalously nonadditive, with the dye absorbance intensity decreasing as the MPC was added. The peculiar acid−base effect was not investigated further.

(31) (a) Häkkinen, H.; Barnett, R. N.; Landman, U. *Phys. Rev. Lett.* **1999**, *82*, 3264−3267. (b) Cleveland, C. L.; Landman, U.; Shafigullin, M. N.; Stephens, P. W.; Whetten, R. L. *Z. Phys. D* **1997**, *40*, 503−508.

(32) From MPC absorbance data gathered by Hicks, J., Guo, R., and Choi, J.-P., UNC-CH.

(33) Thomas, K. G.; Kamat, P. V. *Acc. Chem. Res.* **2003**, *36*, 888−898.

(34) Zhang, J.; Wang, G.; Shon, Y.-S.; Zhou, O.; Superfine, R.; Murray, R. W. *J. Phys. Chem. B* **2003**, *107*, 3726−3732.